Angle-resolved photoelectron spectroscopy of C_{60}

T. Liebsch, O. Plotzke, F. Heiser, U. Hergenhahn, O. Hemmers, R. Wehlitz,
J. Viefhaus, B. Langer, S. B. Whitfield, and U. Becker
Fritz-Haber-Institut der Max-Planck-Gesellschaft, Faradayweg 4-6, D-14195 Berlin, Germany
(Received 1 August 1994; revised manuscript received 28 March 1995)

Angle-resolved photoelectron spectra of gaseous C_{60} were recorded in the photon energy regions from 21 to 108 eV and from 295 to 320 eV. Partial cross sections σ and the angular distribution anisotropy parameter β vary significantly with photon energy, particularly in the near-threshold region of the valence and the core ionization regimes. Some of these effects may be attributed to scattering of the outgoing photoelectron by the atoms of the ionized C_{60} molecule. Our results indicate that the observed satellites of the C(1*s*) main line are most likely of shake-up character. Low-energy electrons emitted below the shake-off threshold indicate the occurrence of *K*-shell vacancy filling double Auger decay.

PACS number(s): 36.40.Mr, 33.80.−b, 33.60.−q

I. INTRODUCTION

After the development of a method [1] for the bulk synthesis of fullerenes, which was discovered in 1985 [2], many studies were performed to investigate the electronic structure of C_{60}. Some of the most common techniques involved are (a) photoelectron spectroscopy (PES) [3–11]; (b) x-ray-absorption spectroscopy (XAS) [10–13]; (c) optical-absorption spectroscopy [1,14–16]; (d) electron-energy-loss spectroscopy (EELS) [17–21]; and (e) inverse-photoemission spectroscopy (IPES) [22].

PES is suitable for the study of occupied electron energy levels, whereas unoccupied states can be investigated by absorption spectroscopy (AS), EELS, and IPES. Progress in theory [23–26] followed experimental advances, giving rise to photoelectron peak designation in terms of molecular orbitals a, t, h, etc. with different symmetries. The commonly used abbreviations HOMO and LUMO mean "highest occupied molecular orbital" and "lowest unoccupied molecular orbital," respectively. For a comparison of optical-absorption spectra with calculated energy level schemes, dipole selection rules have to be taken into account. Due to parity conservation, only dipole transitions between states of different symmetries are allowed.

Although several PES studies have been performed during recent years, none of them has measured partial cross sections and angular distribution parameters of molecular C_{60} as a function of photon energy. Even fixed photon energy studies with discharge lamps did not report any information on the angular distribution of the photoelectrons emitted from C_{60}. In order to determine binding energies, partial cross sections, and angular distributions of the photoelectrons, we recorded angle-resolved spectra in the photon energy regions from $\hbar\omega = 21$ to 108 eV and from 295 to 320 eV. The experiments were carried out in the gas phase.

For atomic and molecular photoionization, the angular-distribution anisotropy parameter β [27] reflects the photoelectron's angular momentum [28]. Knowledge of the β parameter is also useful for correct peak assignments. The angular momentum may be influenced by scattering of the photoelectron in the molecule. This phenomenon is known from shape resonances in molecular photoionization [29].

II. EXPERIMENTAL SETUP

The experiments were performed at the synchrotron radiation facilities in Berlin (BESSY) and Hamburg (HASYLAB) under single-bunch conditions. C_{60} molecules were evaporated by a resistively heated oven running at about $T \sim 600\,^{\circ}\mathrm{C}$ and ionized by monochromatic synchrotron radiation from undulator beamlines, BW3 at HASYLAB and U1 at BESSY, equipped with a plane grating (SX-700) and a toroidal grating monochromator, respectively. The size of the interaction volume was determined by the intersection of the monochromatic photon beam (focal size ~1 mm) with the molecular beam (beam size ~5 mm at about 5 mm above the inlet). In order to determine electron angular distributions, two time-of-flight (TOF) photoelectron spectra were recorded simultaneously at angles of 0° and 54.7° with respect to the polarization vector of the synchrotron light. The degree of linear polarization P_1 of the monochromatic radiation was determined by comparing measured angular distributions of the 2*p* and 2*s* photolines of neon with the data of Krause [30]. The measured values for P_1 were between 0.75 and 0.99; the tilting angle of P_1 was approximately zero degrees. Taking these parameters into account, the angular-distribution parameter of each photoemission peak can be derived from the intensity ratio of the line in the two TOF spectra taken at different angles. Further details of the experimental procedure are given in Ref. [31]. The kinetic-energy resolution of the spectrometers was approximately 2%.

The kinetic-energy calibration of our spectrometer was done using Xe *NOO* Auger and Auger-satellite spectra. In order to calibrate the photon energy of the monochromator, we recorded Ne 2*s*,2*p* photoelectron spectra in the valence ionization region and total-yield electron spectra of CO and N_2 in the core ionization region. The

$1s \rightarrow$LUMO absorption thresholds of these two gases are 287.4 and 401.1 eV, respectively.

III. RESULTS

A. Valence shell ionization

In order to study the partial cross-section behavior, we recorded TOF electron spectra at several photon energies. For this purpose we used the detector at the so-called "magic angle" (54.7°) with respect to the polarization vector of the synchrotron light. The effect of the angular distribution at this position is, in principle, eliminated and relative partial cross sections can be directly determined. The comparison of a gas-phase spectrum with a condensed-phase spectrum, both taken at $\hbar\omega = 65$ eV [Fig. 1(a)], reveals a close similarity, indicating the weakness of the interaction (van der Waals and chemical bonding) between C_{60} molecules in the molecular solid. However, relative intensities of the valence photoemission lines of solid and gaseous C_{60} are different, probably because of inelastic effects and differences in the corresponding transition matrix elements. Note that the theoretical spectrum, a local density calculation [Fig. 1(b)], does not include effects from the variation of these matrix elements. Discrepancies between our experimental spectrum and the calculated density of states in the higher-binding-energy region may be due to satellites or simultaneous double ionization. Above $\hbar\omega \sim 30$ eV, the double-ionization cross section contributes significantly to the total cross section [32,33]; the most probable reason, besides simultaneous double ionization, is valence Auger decay [34].

Only two peaks, HOMO (h_u) and HOMO-1 ($g_g + h_g$) [23], are resolved in the binding-energy spectra. The branching ratios of the two highest occupied orbitals HOMO and HOMO-1, which we obtained by fitting Gaussian line shapes to the spectra, are displayed in Fig. 2. The ratio of the theoretical intensities of the HOMO and HOMO-1 would be 5:9 if the corresponding transition matrix elements were the same for both lines [23]. Benning *et al.* [4] pointed out that transition matrix element effects are influenced by the different symmetries of these two levels. These authors denote HOMO as 1, HOMO-1 as 2, peak *C* as 3, and peak *B* as 4.

The partial cross sections of the two highest occupied levels show minima and maxima at different photon energies, an effect which is less pronounced for the third line, *C*, which is a superposition of several lines. Such an oscillatory structure reminds one of Cooper minima and shape resonances seen in the ionization of heavier atoms. A reason for possible Cooper minima in our case might be the different orbital angular momenta of the electrons in the HOMO and HOMO-1 levels [26]. More likely, however, is the existence of several maxima in the partial cross section generating minimumlike behavior for the limited number of data points in the energy range in this study. Such maxima are seen in a variety of molecules, e.g., in the valence-shell photoionization of CO. They are due to shape resonances with different symmetries in the partial cross section [29]. The mechanism for the occurrence of shape resonances is explained later in the context of core ionization where this effect is more distinctly exhibited.

At this point, we would like to compare our results for free molecules with corresponding measurements on condensed-phase C_{60}. Benning *et al.* [4] report, in their study of the photoemission intensities as a function of

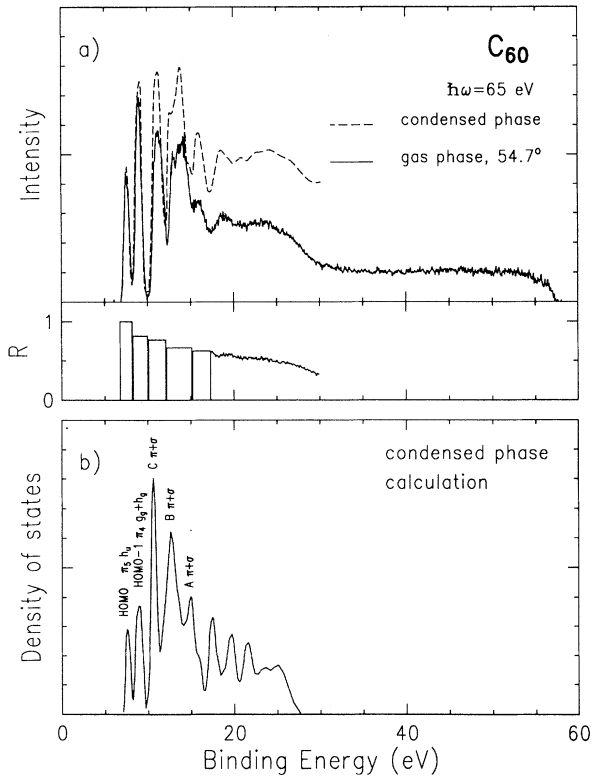

FIG. 1. (a) Valence photoelectron spectra in the condensed [8] and the gas phases taken at a photon energy of 65 eV along with the ratio *R* between the gas- and the condensed-phase photoelectron line intensities. (b) Theoretical spectrum calculated for the condensed phase with peak designations from Ref. [26].

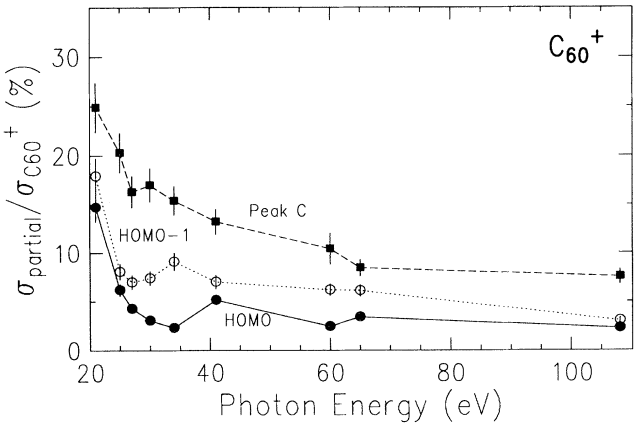

FIG. 2. Branching ratios of the two highest occupied levels and the third line, peak *C*, with respect to the total (single) ionization cross section.

photon energy, remarkable modulations in the partial cross sections. They attribute this behavior to transitions to final states that retain distinct molecular character and symmetry at approximately 100 eV above the highest occupied level. Since they did not record complete spectra, they normalized their results with respect to a peak expected to show little photon-energy-dependent intensity variations due to mixed-symmetry character. In order to compare our results with those of Benning *et al.*, we performed the same type of normalization for our data. The result is shown in Fig. 3. Since peak *B* used for the normalization (peak 4 by Benning *et al.* [4]) is not a completely resolved structure and is on an increasing background function, a direct comparison between the two data sets may be misleading due to different peak analysis procedures. We have therefore renormalized the data of Benning *et al.* by a constant factor of 0.42 in order to bring their relative intensity scale in accord with ours. This procedure does not affect the oscillatory structure seen in the solid-state data and it allows a direct comparison with the gas-phase results. The comparison reveals the same structure of alternating oscillations in the partial cross sections of the two highest occupied molecular orbitals of C_{60} in both the solid and the free molecule although, for the latter, data is much less complete. This shows that the origin of the observed resonance structures should basically be the same. Benning *et al.* compare their results with related work on graphite, which is easier to calculate concerning the wave function in the continuum. For this case, similar effects are expected and were indeed observed [44]. We believe that the existence of nonplanar-wave-like continuum states in the solid is caused by the same scattering effect that gives rise to the occurrence of shape resonances in free molecules. The more pronounced appearance of this effect compared to other molecules, such as CO, results from the larger variety of possible continuum states and the higher number of scattering centers in C_{60}. However, to substantiate this statement, more detailed gas-phase measurements in smaller steps are clearly required.

In order to convert our measured branching ratios into partial cross sections, we used the relative absorption cross-section data of Hertel *et al.* [35]. In spite of the poor agreement between experiment and theory [36–40], we tried to obtain absolute cross sections on the basis of the theoretical calculation [36]. The relative photoabsorption curve of Hertel *et al.*, which was measured via ion yield, was scaled using the theoretical total cross section of $\sigma \sim 140$ Mb at a photon energy of $\hbar\omega \sim 32$ eV [36]. This calibration is rather tentative because to date there exists no experimental verification of these theoretical values; however, for the moment, no better data for absolute calibrations are available. The result is shown in Fig. 4(a).

We also determined the angular distribution of the HOMO and the HOMO-1 for various photon energies, as described above [Fig. 4(b)]. The oscillatory behavior of the anisotropy parameter β at lower photon energies may be explained by scattering of the outgoing photoelectron by other atoms in the molecule, giving rise to shifts in their relative phases. In this sense, the structures seen in σ and β corroborate the shape resonance interpretation. This interpretation is also consistent with the behavior as higher energies are approached, because the scattering probability decreases with increasing photon energy, leveling off asymptotically. The valence shells of each C_{60} molecule consist of σ and π orbitals, which are populated by 180 and 60 electrons per cluster, respectively. In general, the σ orbitals do not seem to exhibit a more anisotropic behavior than the π orbitals, as seen in Fig. 5. At a photon energy of $\hbar\omega = 108$ eV, the corresponding average anisotropies of the $\pi+\sigma$ levels, the σ levels, and the satellites are 0.78, 0.95, and 0.53 ± 0.2, respectively.

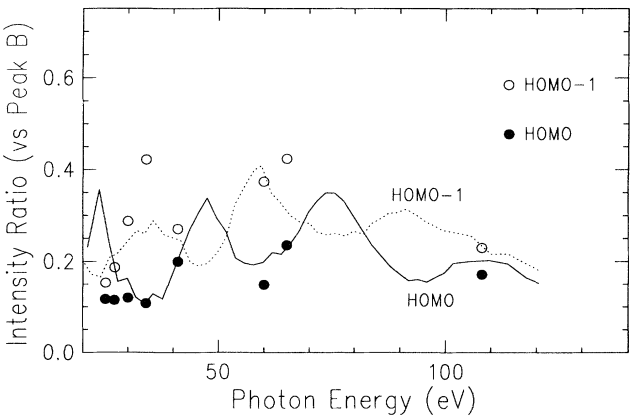

FIG. 3. Comparison of relative peak area ratios with respect to peak *B* with condensed-phase data (solid and dotted line) of Ref. [4]. Our relative error is approximately 10%.

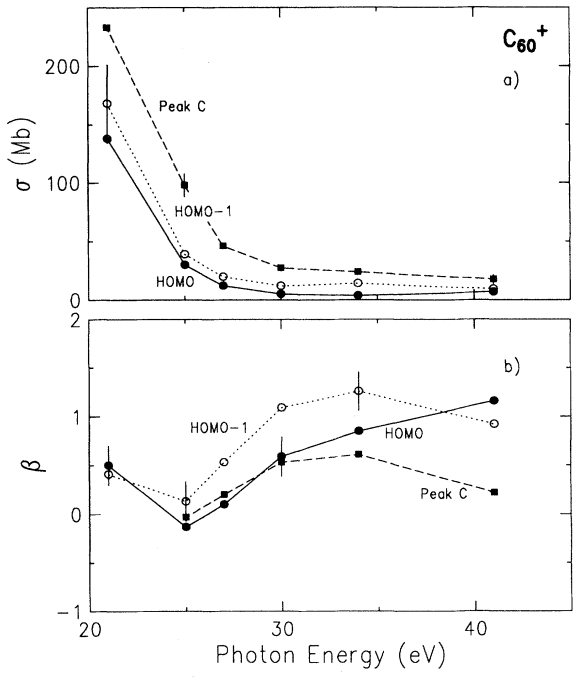

FIG. 4. (a) Partial cross sections of the two highest occupied molecular orbitals (HOMO and HOMO-1) and level *C*, and (b) angular distribution of photoelectrons emitted form these orbitals. See also Fig. 9.

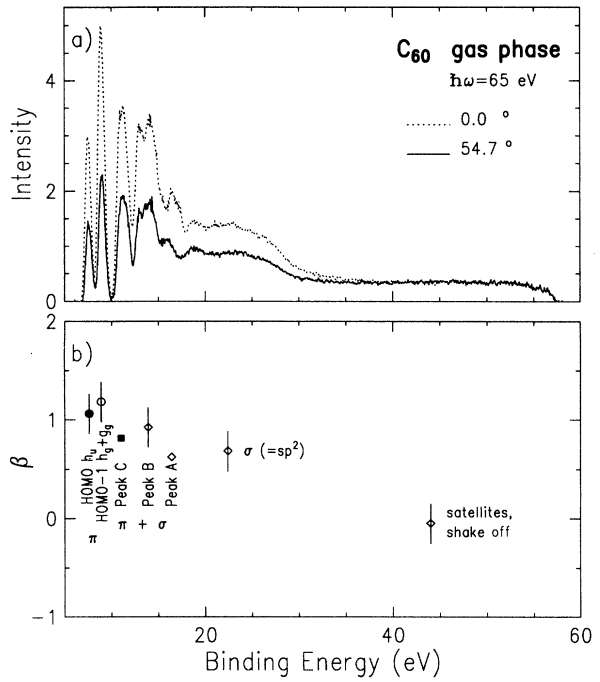

FIG. 5. (a) Photoelectron spectra taken at 65 eV at two different angles; (b) angular-distribution anisotropy parameter β of the different valence-shell photoelectrons.

B. Core ionization

The core photoionization cross section reaches a maximum at a photon energy of $\hbar\omega \sim 300$ eV [11] [Fig. 6(a)]. This absorption spectrum was taken via total electron yield. In order to examine whether or not this maximum is caused by a shape resonance analogous to smaller molecules, we also measured the angular distribution of the $C(1s)$ main line [Fig. 6(b)]. The contribution of valence ionization is negligible in this energy regime, as seen in Fig. 7 (full details given later). The angular-distribution anisotropy parameter β increases with increasing photon energy towards its maximum value $\beta(C1s)=2$. Molecular effects, i.e., deviation of the anisotropy parameter from $\beta=2$, are seen in the energy region between the $C(1s)$ ionization threshold of gaseous C_{60}, $\hbar\omega \sim 290.1$ eV, and about $\hbar\omega \sim 300$ eV. Note that the core binding energies of solid [13] and gaseous [10] C_{60} are the same within the experimental accuracy. In this photon energy region, the photoelectron may be scattered by the atoms in the molecule and thereby pick up additional angular momentum before it finally leaves the molecule. Consequently, the β parameter is lowered from its normal value of two. This shape resonance effect may be explained by the hand waving argument of a simple centrifugal barrier model. The effective potential of the electrons consists of two contributions, the molecular and the centrifugal parts, the latter being strongly influenced by the electron scattering process. The centrifugal barrier forces the electron away from the molecule if its kinetic energy is below $E_{kin} \sim 10$ eV. Therefore, the overlap between the bound core electron and the free electron is decreased at lower kinetic energies. However, when the electron kinetic energy is large enough to overcome the centrifugal barrier, the overlap suddenly increases and the total cross section reaches its maximum at about 10 eV above the $C(1s)$ ionization threshold [29]. Hence, the variation of the β parameter supports the existence of a shape resonance above threshold, similar to carbon in other mole-

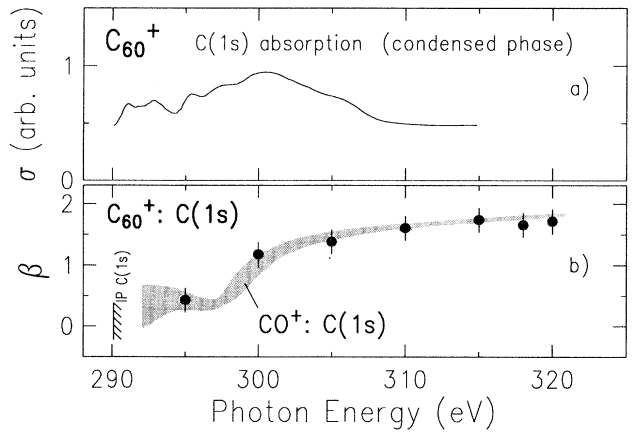

FIG. 6. (a) Photoabsorption cross section above the $C(1s)$ ionization threshold from Ref. [11], and (b) angular distribution of the $C(1s)$ main line of C_{60}, compared with the angular distribution of the CO $C(1s)$ main line [41,42], plotted at the same kinetic energy. Note that the $C(1s)$ ionization potential (IP) of C_{60} is 6.0 eV lower than the IP of CO.

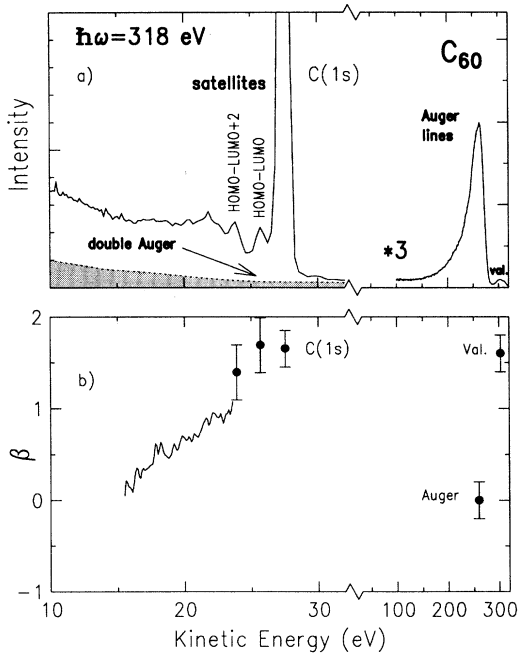

FIG. 7. (a) Photo intensities and Auger line intensities and (b) angular distributions of the $C(1s)$ main line and its satellites. The shaded area in (a) represents the low-energy part of the double-Auger continuum. The threshold kinetic energy for the high-energy part of the double-Auger continuum is assumed to be 10 eV below the corresponding diagram lines.

cules, e.g., CO [Fig. 6(b)] [41, 42].

In addition to the $C(1s)$ main line, satellites are seen in the photoelectron spectrum (Fig. 8). To infer additional information about the resolved satellites, we also measured their angular distributions. Their anisotropy parameter β does not differ significantly from the β parameter of the main line (Fig. 7). These satellites are most likely to result from shake-up processes without any angular-momentum transfer (i.e., monopole excitations). The first satellite with a binding energy of 1.9 eV corresponds to a HOMO→LUMO transition. The second satellite with a binding energy of 3.8 eV is assigned as a HOMO→LUMO+2 transition (Fig. 7), according to Enkvist *et al.* [9]. The Hückel symbols of the LUMO (t_u), LUMO+1(t_{1g}), LUMO+2(t_{2u}), and LUMO +3(h_g) may be found in Ref. [25]. In contrast to our results, Weaver *et al.* [8], who compare their satellite spectrum (Fig. 8, bottom) with EELS spectra, denote the second satellite as a dipole transition (HOMO→LUMO +3). Monopole excitations are suppressed in EELS if the initial electron energy greatly exceeds the excitation energy. According to Krummacher *et al.* [10], dipole contributions to this satellite should be significant. Their assignment of the second satellite is HOMO→LUMO+2 and LUMO+3. Following Weaver's interpretation, the second satellite should show an approximately isotropic angular distribution, as one would expect for a conjugate shake-up satellite, because no angular momentum is transferred to the photoelectron. Furthermore, the relative intensity of conjugate shake-up satellites (with respect to the main line) decreases with increasing photon energy due to the decreasing overlap between bound-state and continuum wave functions. We compared the measured relative intensity of the first two satellites ($\hbar\omega = 318$ eV) with Krummacher's results ($\hbar\omega = 390$ eV). The intensities of the first two satellites in these spectra are nearly the same within the experimental accuracy, supporting an interpretation of this satellite as a shake-up line. The β-parameter curve of the other (nonresolved) satellites in Fig. 7 indicates a tendency to smaller β values, perhaps due to scattering at lower kinetic energies as seen for the $C(1s)$ main line. To prove this interpretation, further measurements at higher photon energies are necessary.

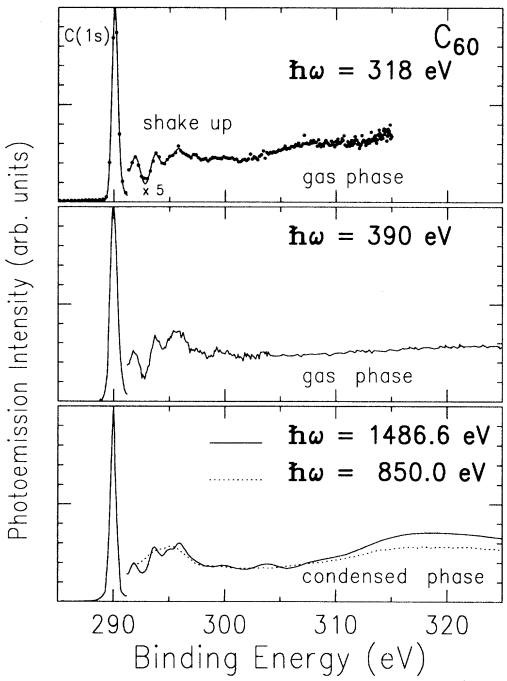

FIG. 8. Comparison of our $C(1s)$ gas-phase satellite spectrum with the gas-phase spectrum of Krummacher *et al.* [10] taken at a photon energy of 390 eV and two corresponding spectra recorded in the condensed phase [8,10] at photon energies of 1486.6 and 850 eV, respectively.

Concerning the $C(1s)$ satellite spectrum (Fig. 8), the broad peak at a binding energy of about 30 eV leads us to some questions about its origin and intensity. This peak could be due to inelastic scattering [9], plasmon excitation [8], photoelectron satellites, or a continuous distribution of electrons such as shake-off and double Auger. In principle, all of these mechanisms could contribute to our observed spectrum. Therefore, we will discuss the different possibilities briefly on a more quantitative basis beginning with inelastic scattering. The large uncertainty in the determination of the target density in the interaction volume results from the oven temperature measurement due to the difficulties in mounting the thermocouple directly in the inner part of the oven where the evaporation takes place. The measured temperature should therefore be regarded with some caution. In order to estimate the target density somewhat quantitatively, a count-rate comparison between CO and C_{60} will be more reliable if the core ionization cross sections are of the same order of magnitude [45]. The target pressure for our CO measurements was less than 0.1 Pa [41]. The $C(1s)$ photoelectron count rate, which was normalized to the photon flux, was 20% higher than in the case of C_{60}, suggesting a similar carbon target density in both cases. Taking into account the molecular-size dependence of inelastic scattering, this scattering effect may indeed contribute to our spectrum. However, the corresponding inelastic scattering peaks in CO are relatively weak, even in the case of 10^2-10^3 times larger sample pressures as used, e.g., by the electron-spectroscopy-for-chemical-analysis (ESCA) measurement of Gelius [46]. These scattering peaks account for several percent of the total shake-up structure. We assume similar contributions in our spectrum due to the smaller density but larger size of the molecule. The estimated ratio of the target densities of solid and gaseous C_{60} is, under the above assumptions, at least 10^7 at the interaction volume. The dominant part of the observed peak structure results, therefore, from intrinsic processes such as shake-up and plasmon excitation, whereas extrinsic contributions such as inelastic scattering are virtually negligible. We will return to this point later.

In the context of this more technical discussion, we want to concentrate now on possible continuous energy distributions of electrons. Here we have to distinguish between shake-off and double Auger, both of them having maximum intensity at very low kinetic energy. Both pro-

cesses are indistinguishable at higher excess energies, such as in the case of our spectrum recorded at $\hbar\omega = 318$ eV. However, a spectrum taken at $\hbar\omega = 295$ eV should be free from shake-off contributions associated with $C(1s)$ photoionization because it is below any corresponding threshold that we could tentatively assume (~ 301 eV). The observed distribution of low-energy electrons at this energy should therefore be solely due to double-Auger processes, which are known from most K-shell vacancy-filling processes, both resonant and nonresonant ones. Double-Auger decay contributes to about 10% of the total Auger intensity in the rare gases [47] and is assumed to contribute as much as 60% of all Auger processes following $4d$ shell ionization of atomic barium [48]. Our estimate of the double-Auger probability ($34^{+2}_{-11}\%$) in C_{60} is the average of all spectra above 310 eV but coincides basically with the spectrum taken at $\hbar\omega = 318$ eV with the best signal-to-noise ratio. This is a relatively high number, which has to be proved independently, for example by complementary methods such as photoion mass spectrometry. The shaded area in Fig. 7 shows the normalized double-Auger intensity underneath the satellite and plasmon peaks. The corresponding $C(1s)$ spectrum shown in Fig. 8 is a difference spectrum where the double-Auger contribution was subtracted in order to facilitate comparison with other spectra taken at higher energies where these two contributions (double Auger and satellite intensities) are clearly separated.

We return now to the interpretation of the broad structure in the satellite spectrum at a binding energy of about 30 eV. Weaver *et al.* [8] and Krummacher *et al.* [10] suggested that this satellite could be caused by a plasmon excitation. Enkvist *et al.* [9] proposed another mechanism related to resonant processes. In the following we discuss the implications that result from our arguments. In metals (collective) plasmon satellites are much weaker than usual photoemission satellites, and the relative plasmon intensity (with respect to the main line) should rise with increasing photon energy [43]. This effect is shown by the two solid-state spectra taken at higher photon energies with respect to each other, but also with respect to the gas-phase spectrum taken by Krummacher *et al.* at $\hbar\omega = 390$ eV. However, the estimated satellite intensity of our gas-phase spectrum taken at even lower photon energy seems to be similar or even higher compared to the corresponding intensity in the spectrum of Krummacher *et al.* [10], in contrast to the hypothesis of decreasing intensity toward threshold. This behavior requires further examination in future photon-energy-dependent experiments in order to determine the energy dependence of the broad satellite peak more precisely. Comparing with solids $C(1s)$ satellite spectra of graphite and diamond [49] show features similar to the two plasmon satellites of C_{60} [8]. Following the argument of McFeely *et al.* [49], these peaks may also consist of usual photoelectron satellites rather than being pure plasmon satellites. In addition to plasmon excitation, internal scattering of the photoelectron on its way out, as is known from satellites at low kinetic energies [50] and virtual molecular states corresponding to shape resonances, might also contribute to the observed broad structure in the photoelectron spectrum, in particular near threshold [51].

Finally we looked for angular distribution effects in the KVV-Auger spectra. Under the conditions of recording low-resolution Auger spectra, we found no evidence of an anisotropic Auger emission above the $C(1s)$ ionization threshold ($\beta \sim 0$, see Fig. 7), indicating little or no anisotropy of the preceding photoabsorption process. However, high-resolution measurements are necessary to prove this statement, as is found in the case of CO [52].

C. Partial and total cross sections

Partial and total cross sections are plotted in the photon energy region from the first ionization threshold ($V_{\text{ion}} = 7.61$ eV) to $\hbar\omega \sim 315$ eV [Fig. 9(a)]. The relative-absorption curve of Hertel *et al.* [35] was scaled, assuming the theoretical cross section to be $\sigma \sim 140$ Mb at a photon energy of $\hbar\omega \sim 32$ eV, according to Wendin and Wästberg [36]. The ratio of core-to-valence ionization cross section was obtained, determining the KVV Auger to valence PES peak area ratio (36.5:1) at a photon energy of $\hbar\omega = 315$ eV, yielding an extrapolated cross section of about $\sigma \sim 2$ Mb. Following Wendin's calculation based on the jellium model [36], the total cross section of the C_{60} cluster seems to be smaller than the cross section of the CO molecule [41] in the photon energy region between $\hbar\omega \sim 120$ eV and the $C(1s) \rightarrow$LUMO absorption threshold, a result that is somewhat puzzling. In spite of this, we have extrapolated this theoretical data to higher energies by assuming an asymptotic behavior of the valence photoionization $\sigma \sim (\hbar\omega)^{-7/2}$ because no other data were available for this purpose. However, more elaborate theoretical work is necessary to explore the behavior of the partial cross sections quantitatively. The behavior of the corresponding angular-distribution parameter β over the whole energy range is shown in Fig. 9(b).

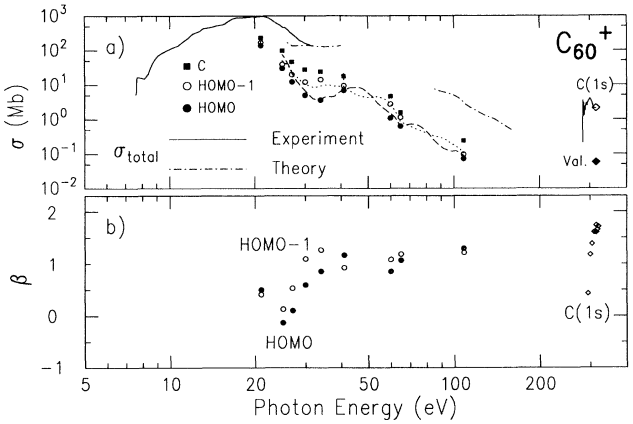

FIG. 9. (a) Partial cross sections for valence and inner-shell photoionization, using the experimental data of Hertel *et al.* [35] (valence ionization) and Schlögl *et al.* (core ionization) [11] for the total cross sections and the theory of Wendin and Wästberg [36] for absolute calibration. The dashed and the dotted lines represent the solid state data from Ref. [4], normalized to our peak B intensities. (b) Angular-distribution anisotropy parameters of two valence lines and the $C(1s)$ line.

IV. SUMMARY

Angle-resolved photoelectron spectra of gaseous C_{60} were recorded. Partial cross sections and angular distributions show significant variations in the valence ionization as well as in the core ionization regions, especially in the kinetic-energy range from 0 to 20 eV above threshold. Some of these effects may be explained on the basis of scattering of the outgoing photoelectrons by the atoms of the spherical-shaped molecule. Towards higher photon energies the partial cross sections show oscillatory behavior similar to the occurrence of shape resonances and Cooper minima in atoms, being interpreted primarily in terms of shape resonances in the corresponding partial cross sections in good accord with the condensed-phase data. The clear appearance of these oscillating resonances in the absolute partial cross sections below 30 eV is partly masked by the occurrence of the "giant plasmon resonance" and the limited number of photon energies at which the partial cross sections were examined. The satellites of the $C(1s)$ main line appear to be mostly shake-up satellites; no particular indication for conjugate shake-up behavior could be found. Total $C(1s)$ photoelectron and Auger intensities are approximately equal, assuming a double-Auger rate of approximately 34%.

ACKNOWLEDGMENTS

This work was supported by the Bundesministerium für Bildung, Wissenschaft, Forschung and Technologie under Contract No. 05 5EBFXB2. S.B.W. is indebted to the Humboldt Foundation, F.H. to the Deutscher Akademischer Austauschdienst, and U.H. to the Senate of Berlin for financial support.

[1] W. Krätschmer, L. Lamb, K. Fostiropoulos, and D. Huffman, Nature **347**, 354 (1990).
[2] H. Kroto, J. Heath, S. O'Brien, R. Curl, and R. Smalley, Nature **318**, 162 (1985).
[3] D. Lichtenberger, M. Jatcko, K. Nebesny, C. Ray, D. Huffman, and L. Lamb, Mat. Res. Soc. Symp. Proc. **206**, 673 (1991); D. Lichtenberger, K. Nebesny, C. Ray, D. Huffman, and L. Lamb, Chem. Phys. Lett. **176**, 203 (1991).
[4] P. Benning, D. Poirer, N. Troullier, J. Martins, J. Weaver, R. Haufler, L. Chibante, and R. Smalley, Phys. Rev. B **44**, 1962 (1991).
[5] S. Molodtsov, A. Gutierrez, M. Domke, and G. Kaindl, Europhys. Lett. **19**, 369 (1992).
[6] P. Brühwiler, A. Maxwell, A. Nilsson, R. Whetten, and N. Martensson, Chem. Phys. Lett. **193**, 311 (1992).
[7] C. Chen, L. Tjeng, P. Rudolf, G. Meigs, J. Rowe, J. Chen, J. McCauley, A. Smith, A. McGhie, W. Romanow, and E. Plummer, Nature **352**, 603 (1991).
[8] J. Weaver, Y. Chen, T. Ohno, G. Kroll, and R. Smalley, Phys. Rev. Lett. **66**, 1741 (1991); P. Benning, D. Poirer, T. Ohno, Y. Chen, M. Jost, F. Stepniak, G. Kroll, J. Weaver, J. Fure, and R. Smalley, Phys. Rev. B **45**, 6899 (1992); J. Weaver, J. Phys. Chem. Solids **53**, 1433 (1992).
[9] C. Enkvist, S. Lunell, B. Sjörgren, S. Svensson, P. Brühwiler, A. Nilsson, A. Maxwell, and N. Martensson, Phys. Rev. B **48**, 14 629 (1993).
[10] S. Krummacher, M. Biermann, M. Neeb, A. Liebsch, and W. Eberhardt, Phys. Rev. B **48**, 8424 (1993); M. Biermann, Ph.D. thesis, Universität zu Köln, 1994.
[11] H. Werner, T. Schedel-Niedrig, M. Wohlers, D. Herein, B. Herzog, R. Schlögl, M. Keil, A. M. Bradshaw, and J. Kirschner, J. Chem. Soc. Faraday Trans. **90**, 403 (1994).
[12] L. Terminello, D. Shuh, F. Himpsel, D. Lapiano-Smith, J. Stöhr, D. Bethune, and G. Meier, Chem. Phys. Lett. **182**, 491 (1991).
[13] P. Brühwiler, A. Maxwell, P. Rudolf, C. Gutleben, B. Wästberg, and N. Martensson, Phys. Rev. Lett. **71**, 3721 (1993).
[14] H. Ajie, M. Alvarez, S. Anz, R. Beck, F. Diederich, K. Fostiropoulos, D. Huffman, W. Krätschmer, Y. Rubin, K. Schriver, D. Sensharma, and R. Whetten, J. Phys. Chem. **94**, 8630 (1990).
[15] A. Hebard, R. Haddon, R. Fleming, and A. Kortan, Appl. Phys. Lett. **59**, 2109 (1991).
[16] B. Brady and E. Beiting, J. Chem. Phys. **97**, 3855 (1992); Q. Gong, Y. Sun, Z. Huang, X. Zhu, Z. Gu, and D. Quiang, J. Phys. B **27**, L199 (1994).
[17] G. Gensterblum, J. Pireaux, P. Thiry, R. Caudano, J. Vigneron, P. Lambin, A. Lucas, and W. Krätschmer, Phys. Rev. Lett. **67**, 2171 (1991).
[18] V. Dravid, S. Liu and M. Kappes, Chem. Phys. Lett. **185**, 75 (1991).
[19] E. Sohmen, J. Fink, and W. Krätschmer, Z. Phys. B **86**, 87 (1992).
[20] C. Bulliard, M. Allan and S. Leach, Chem. Phys. Lett. **209**, 434 (1993); J. Keller and M. Coplan, Chem. Phys. Lett. **193**, 89 (1992).
[21] P. Kovarik, E. Bourdon, and E. Prince, Phys. Rev. B **49**, 7744 (1994).
[22] M. Jost, N. Troullier, D. Poirer, J. Martins, J. Weaver, L. Chibante, and R. Smalley, Phys. Rev. B **44**, 1966 (1991).
[23] R. Haddon, L. Bruns, and K. Raghavachari, Chem. Phys. Lett. **125**, 459 (1986).
[24] S. Saito and A. Oshiyama, Phys. Rev. Lett. **66**, 2637 (1991).
[25] C. White, in *Buckminsterfullerene,* edited by J. W. Billups and M. Ciufolini (VCH, Weinheim, 1993), p. 139.
[26] N. Troullier and J. Martins, Phys. Rev. B **46**, 1754 (1992); J. Martins, N. Troullier and J. Weaver, Chem. Phys. Lett. **180**, 475 (1991).
[27] C. Yang, Phys. Rev. **74**, 764 (1948).
[28] J. Cooper and R. Zare, J. Chem. Phys. **48**, 942 (1968); U. Fano and D. Dill, Phys. Rev. A **6**, 185 (1972).
[29] J. Dehmer and D. Dill, Phys. Rev. Lett. **35**, 213 (1975).
[30] M. Krause, in *Synchrotron Radiation Research,* edited by H. Winick and S. Doniach (Plenum, New York, 1980), p. 121.
[31] U. Becker, D. Szostak, H. G. Kerkhoff, M. Kupsch, B. Langer, R. Wehlitz, A. Yagishita, and T. Hayaishi, Phys. Rev. A **39**, 3902 (1989).
[32] R. Yoo, B. Rusic, and J. Berkowitz, J. Chem. Phys. **96**, 911 (1992).
[33] T. Drewello, W. Krätschmer, M. Fieber-Erdmann, and A. Ding, Int. J. Mass Spectrosc. Ion Processes **124**, R1 (1993).
[34] U. Becker, O. Hemmers, B. Langer, A. Menzel, R. Wehlitz, and W. Peatman, Phys. Rev. A **45**, 1295 (1992).

[35] I. Hertel, H. Steger, J. de Vries, B. Weisser, C. Menzel, B. Kamke, and W. Kamke, Phys. Rev. Lett. **68**, 784 (1992).
[36] G. Wendin and B. Wästberg, Phys. Rev. B **48**, 14 764 (1993).
[37] G. Bertsch, A. Bulgac, D. Tomanek, and Y. Wang, Phys. Rev. Lett. **67**, 2690 (1991).
[38] M. Puska and R. Nieminen, Phys. Rev. A **47**, 1181 (1993).
[39] M. P. Lambin, A. Lucas, and J. Vigneron, Phys. Rev. B **46**, 1794 (1992).
[40] D. Östling, P. Apell, and A. Rosen, Europhys. Lett. **21**, 539 (1993).
[41] O. Hemmers, Ph.D. thesis, Technische Universität Berlin, 1993; O. Hemmers, *Korrelationseffekte in kleinen Molekülen,* Studies of Vacuum Ultraviolet and X-ray Processes Vol. 3, edited by U. Becker (AMS, New York, 1993).
[42] M. Schmidbauer, A. L. D. Kilcoyne, H. M. Köppe, and J. Feldhaus, in *Proceedings of the International Workshop on Photoionization, Berlin, 1992,* edited by U. Becker and U. Heinzmann (AMS, New York, 1993), p. 161.
[43] C. Almbladh and L. Hedin, in *Handbook on Synchrotron Radiation,* edited by E.-E. Koch (North Holland, Amsterdam, 1983), p. 839.
[44] A. Bianconi, S. Hagström, and R. Bachrach, Phys. Rev. B **16**, 5543 (1977).
[45] M. Ya. Amusia, I. Lee, and V. Kilin, Phys. Rev. A **45**, 4576 (1992).
[46] U. Gelius, J. Electron Spectrosc. Relat. Phenom. **5**, 985 (1974).
[47] T. Carlson and M. Krause, Phys. Rev. Lett. **14**, 390 (1965); **17**, 1079 (1966).
[48] S. Baier, G. Gottschalk, T. Kerkau, T. Luhmann, M. Martins, M. Richter, G. Snell, and P. Zimmermann, Phys. Rev. Lett. **72**, 2847 (1994).
[49] F. McFeely, S. Kowalczyk, L. Ley, R. Cavell, R. Pollak, and D. Shirley, Phys. Rev. B **9**, 5268 (1974).
[50] J. Tulkki, Phys. Rev. Lett. **62**, 2817 (1989).
[51] U. Becker and D. Shirley, Phys. Scr. **T31**, 56 (1990).
[52] O. Hemmers, F. Heiser, J. Eiben, R. Wehlitz, and U. Becker, Phys. Rev. Lett. **71**, 987 (1993).